Polymer Bulletin
https://doi.org/10.1007/s00289-022-04261-8

ORIGINAL PAPER

Corrosion and the antibacterial response of epoxy coating/drug-loaded mesoporous silica

Mahdi Yeganeh[1] · Taher Rabizadeh[2] · Mohammad Sajad Rabiezadeh[1] · Maryam Kahvazizadeh[1] · Hossein Ramezanalizadeh[3]

Received: 1 September 2021 / Revised: 6 April 2022 / Accepted: 25 April 2022

Abstract
The present study aims to investigate the loaded mesoporous silica with sulfamethazine and the effect of its dispersion in the epoxy coating on the corrosion behavior of coated mild steel. The composite coating was synthesized by mixing 1wt. % mesoporous silica without (Mes) and with sulfamethazine (Mes-S) and an epoxy polymer. Electrochemical impedance spectroscopy (EIS), field emission scanning electron microscopy (FESEM), and X-ray photoelectron spectroscopy (XPS) were used to analyze corrosion resistance of the epoxy coating containing Mes and Mes-S. Results revealed the higher corrosion resistance of epoxy/Mes-S in the NaCl solution after 1000 h of immersion compared to epoxy/Mes, indicating higher barrier behavior of epoxy/Mes-S due to the inhibition effect of sulfamethazine. Specifically, epoxy/Mes-S exhibited a R_{ct} of 67 kΩ cm^2 after 1000 h of immersion, while the epoxy/Mes and epoxy showed R_{ct} of 9.8 and 7 kΩ cm^2, respectively. Besides, it was shown that the epoxy/Mes-S coating could inhibit the growth of E. coli as the antibacterial coating due to the effect of sulfamethazine on the bacteria.

Keywords Mesoporous silica · Sulfamethazine · Epoxy coating · Corrosion · Antibacterial agent

✉ Mahdi Yeganeh
m.yeganeh@scu.ac.ir

[1] Materials Science and Engineering, Faculty of Engineering, Shahid Chamran University of Ahvaz, Ahvaz, Iran

[2] Department of Materials Engineering, Faculty of Mechanical Engineering, University of Tabriz, Tabriz 51666-16471, Iran

[3] Department of Materials and Polymer Engineering, Faculty of Engineering, Hakim Sabzevari University, P.O. Box 397, Sabzevar, Iran

Published online: 17 May 2022

Introduction

The application of polymeric coatings on metal substrates is known as one of the conventional methods to minimize corrosion damage observed in many industries [1–7]. However, poor structural integrity and lack of durability against corrosive ions are key disadvantages of these coatings. A promising approach to resolving this issue is to introduce inert active corrosion inhibitors into the polymeric matrix [8, 9]. Consequently, it is in recent years that the encapsulation of corrosion inhibitor molecules in micro- or nano-containers before their incorporation into the coating and the synthesis of an intelligent coating has been invented [10]. It can be said that the applied containers are the main part of the smart coating that releases the encapsulated corrosion inhibitors when the pH and/or potential change in the corrosive area [11–14].

The carriers in the smart coatings are supposed to possess certain features such as environmental stability, compatibility with the coating matrix, and the ability to release the corrosion inhibitor [11, 15]. Among several types of containers, mesoporous silica has received a special interest for its ordered hexagonal structure, high value of surface areas and pore volumes, good resistance to thermal and chemical shocks, remarkable biocompatibility, and adjustable chemistry for functionalization [16–20]. Many researchers have noted the potential of this inorganic material to be used as a container for corrosion inhibitor molecules [8, 11, 21, 22]. Some of them have applied mesoporous silica without any modification and loaded the inhibitor directly into the structural pores [21]. On the other hand, the modification and functionalization of mesoporous silica have also been studied, and a decrease in the active sites of mesoporous was observed due to reaction with the functional groups of the molecules or unwanted leakage of the inhibitor from the pores of mesoporous silica [8, 11].

Many types of inorganic and organic corrosion inhibitors have been utilized to be loaded in the pores of mesoporous silica [23–26]. Mesoporous silica has been loaded with the different types of inhibitor including organic, inorganic, and complex compounds. Organic molecules are the most commonly applied inhibitor type in this classification. Mesoporous silica suspension was usually mixed with the aqueous or organic solution of inhibitor [27]. However, most of the utilized organic inhibitors are expensive and may be toxic [21, 22]. Sulfa drugs with $–NH_2$ group, $–SO_2–NH–$ group, O and/or N heteroatoms, and aromatic rings functional groups in their molecular structures are low-cost, eco-friendly compounds that revealed desired green corrosion inhibition performance in the corrosive media [28, 29]. This drug is one of the oldest classes of synthetic antibiotics that are still prescribed in medicine nowadays [30]. The heterocyclic antibiotic sulfamethazine is an important antibiotic. Due to its low cost and broad spectrum of antibacterial properties, it is one of the most widely used antibiotics in the world [31]. However, its degradation in the environment by traditional biological treatment methods is of challenge [32].

Mesoporous materials can be applied as remarkable carriers for different types of drugs including sulfa drugs [33–35]. However, there are rare reports describing

the loading of sulfa drug into the mesoporous silica to obtain a carrier for corrosion protection and antibacterial application [36]. Asadi and her co-workers have loaded a sulfa drug in a mesoporous silica carrier and embedded it in a polymer coating. They found that the presence of sulfa drug could enhance corrosion protection of coating in the 3.5 wt.% NaCl after 30 days of immersion [36]. In this work, mesoporous silica suspension was loaded with sulfamethazine under a reduced pressure. Then, composite epoxy/sulfamethazine-loaded mesoporous silica was prepared. In this study, a drug molecule (sulfamethazine) was loaded into mesoporous silica and studied for its effect on mesoporous silica characterization and performance. The characterizations of the mesoporous silica powders after immersion at the different pHs were investigated by Brunauer–Emmett–Teller (BET), field emission scanning electron microscopy (FESEM), X-ray diffraction (XRD), and Fourier transform infrared spectroscopy (FTIR) techniques to find out proper solution. The corrosion resistance efficiency of the produced composite epoxy coating containing drug-loaded mesoporous silica in the 0.05 M NaCl solution was studied using electrochemical impedance spectroscopy (EIS), electrochemical noise (EN), FESEM, and X-ray photoelectron spectroscopy (XPS). Additionally, the antibacterial performance of mesoporous silica loaded with sulfamethazine was evaluated compared to the blank mesoporous silica.

Experimental procedures

Materials

Hexadecyltrimethylammonium bromide ($C_{19}H_{42}BrN$, 99%), tetraethylorthosilicate ($SiC_8H_{20}O_4$, 98%), and sulfamethazine ($C_{12}H_{14}N_4O_2S$, 99%) were purchased from Sigma-Aldrich. Hydrochloric acid (HCl) with 37% purity, NaCl, and NaOH was obtained from Mojallali Co. Iran without any further purification. The steel specimens with dimensions of $10 \times 10 \times 0.1$ cm were provided from Foolad Mobarakeh Co. with a chemical composition of 0.5% Mn, 0.05% S, 0.12% C, 0.046% P, 0.32% Si, and balanced Fe (in weight. %). The solutions were prepared using double-distilled water.

Methods

Coating synthesis

In a similar manner to previous studies, mesoporous silica powders and mesoporous silica loaded with sulfamethazine were synthesized [36, 37]. These powders are now referred to as Mes (unloaded mesoporous silica) and Mes-S (sulfamethazine-loaded mesoporous silica). Low carbon steel plates were ground with SiC sandpapers from 100 to 1200 grit, degreased with acetone, rinsed with water, and finally dried in the air. An epoxy resin with the approximate equivalent weight of 500 was mixed with the appropriate amount of toluene. The epoxy containing 1 wt.% Mes or Mes-S was

homogenized for 1 h and ultrasonically stirred for 10 min. The mixture was then applied using a film applicator to steel plates with a thickness of 50 ± 5 μm. Finally, the coatings were placed in an oven at 80 °C for 45 min. Three types of blank epoxy coating, epoxy coating containing Mes, and epoxy coating with Mes-S were produced and labeled as Ep, Ep/Mes, and Ep/Mes-S, respectively.

Characterization of Mes and Mes-S

A scanning electron microscope (Field-Emission; CamScan Mira; 15 kV) equipped with an energy dispersive X-ray spectroscopy (EDS) detector was used to evaluate the size and morphology of Mes and Mes-S powders. Low-angle X-ray diffraction tests were performed in the range of 1–10° with a Philips X'Pert MPD diffractometer (Cu Kα source) to estimate the pore size diameter of synthesized powders. The specific surface area, average pore diameter, and the pore volume were measured using an adsorption–desorption isotherm (liquid N_2, BELSORP mini-II; Belsorp; Japan). Fourier transforms infrared (FTIR) technique (Nicolet IR 100) was also performed in the wavelength range from 4000 to 500 cm^{-1}.

Corrosion performance of the coating

Electrochemical impedance spectroscopy (EIS) was used to examine the corrosion performance of epoxy composite coatings in 0.05 M NaCl solutions. A resin matrix had been used to mount the samples, so only 1 cm^2 of surfaces were exposed to the corrosive solution. Measurements were conducted at 25 °C under open circuit potential conditions. Next, a three-electrode configuration including a saturated silver/silver chloride reference electrode, a Pt counter electrode, and a working electrode (i.e., the produced Ep, or Ep/Mes, or Ep/Mes-S coatings) was utilized. The EIS analyses were conducted at 10^{-2}–10^5 Hz and after immersing the working electrodes in the 0.5 M NaCl solution for 10 and 1000 h. The EIS data were recorded using an AUTOLAB PGSTAT 30 potentiostat equipped with NOVA software. Each experiment was repeated three times to ensure the accuracy. ZView software was used for EIS data fitting [38]. A fast Fourier transform (FFT) was used to transform the potential and current noise data collected in the time domain to the frequency domain. After 1000 h of immersion, electrochemical noise data were collected for 512 s.

Characterization of the coatings

An EDS detector was used to study the oxygen and sulfur distribution in Ep/Mes-S coating. The chemical state of the corroded area was investigated using X-ray photoelectron spectroscopy (XPS) with an Al K anode at 1486.6 eV after scratching the surface of Ep/Mes-S coating and immersing it in 0.05 M NaCl for 10 h.

Antibacterial activity

The diffusion disk test was conducted to evaluate the antibacterial properties of mesoporous silica loaded with sulfamethazine in diluted chloride media. In a Petri dish, 1 mL of *Escherichia coli* (*E. coli*) bacterial suspension was added onto a solid growth medium. 10 ml of agar solution was poured into sterile Petri dishes followed by 15 ml of seeded medium previously inoculated with bacterial suspension to provide a 10^5 CFU/ml solution. Three sterile paper disks with a diameter of 6 mm were placed on top of each agar plate. Before this stage, one disk was permeated with 20 µL of the solution with released sulfamethazine from mesoporous silica in the diluted chloride media. Another disk was impregnated without sulfamethazine. The third disk served as the control specimen and was impregnated with an antibiotic drug. These plates were kept in the fridge at 5 °C for 2 h and then incubated at 35 °C for 24 h. Finally, a ruler with a 1 mm resolution was used to measure the width of inhibition zones, which were regarded as indicators of antibacterial activity. Besides, fluorescent microscopy (OLYMPUS) was applied to show the presence of *E. coli* after attachment on the samples.

Results and discussion

Mesoporous silica characterization

Figure 1 presents a micrograph of the as-produced mesoporous silica (MS) powder. The synthesized particles (about 100 nm in diameter) had an elongated worm shape due to the high concentration of structural water [39]. As a result of hydrolyzing

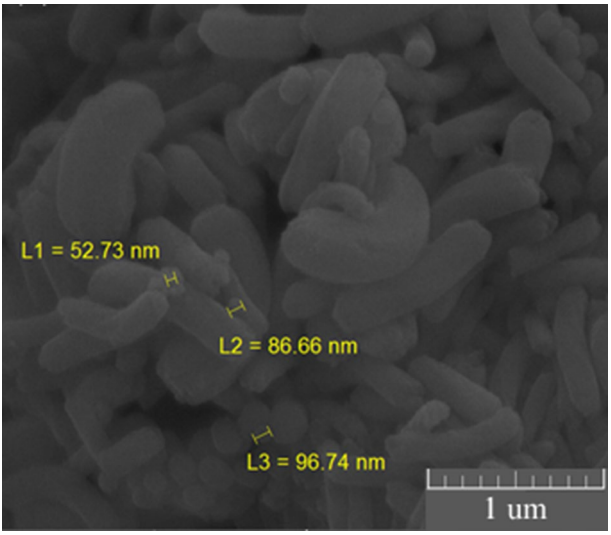

Fig. 1 FESEM morphology of the produced mesoporous silica

TEOS molecules during the mesoporous silica synthesis stage, the molecules only attach to a preformed droplet and grow preferentially onto the nucleus in a single orientation [40]. The length of the particles was in the range of 200 nm to 1 µm.

N_2 adsorption/desorption test was conducted before and after immersion of the powders in the corrosive solutions of 0.05 M NaCl, 1 M HCl, or 1 M NaOH to understand the effects of pH values on the structural integrity of the particles as shown in Fig. 2. The results indicate that mesoporous silica (MS) displayed a typical type IV isotherm before immersion, as well as a distinct hysteresis loop of H_2 in the range of 0.4–1.0 P/Po (P is the partial pressure and Po is the saturated vapor pressure of the adsorbate [41]). Furthermore, the specific surface area, the pore volume, and the average diameter of the MS powder were measured to be 881.1 $m^2\ g^{-1}$, 0.65 $cm^3\ g^{-1}$, and 2.9 nm, respectively. When MS was immersed in NaCl, HCl, and NaOH solutions, the surface area values decreased to 521, 254.5, and 81.5 $m^2\ g^{-1}$, respectively, indicating a reduction of active surfaces caused by reaction with the solution species. Moreover, a type II isotherm was obtained for MS exposed to the alkaline solution, suggesting the nonporous or macroporous nature of the adsorbent. This isotherm also represents the adsorption on open surfaces, mainly resulting from the destruction of mesoporous silica [41]. This means that mesoporous silica has lost its ordered structure in the alkaline media due to the breakdown of the Si–O–Si structure in the high-pH solution [36, 42]. Other solutions, however, resulted in a reduction of surface area, but mesoporous structure did not deteriorate.

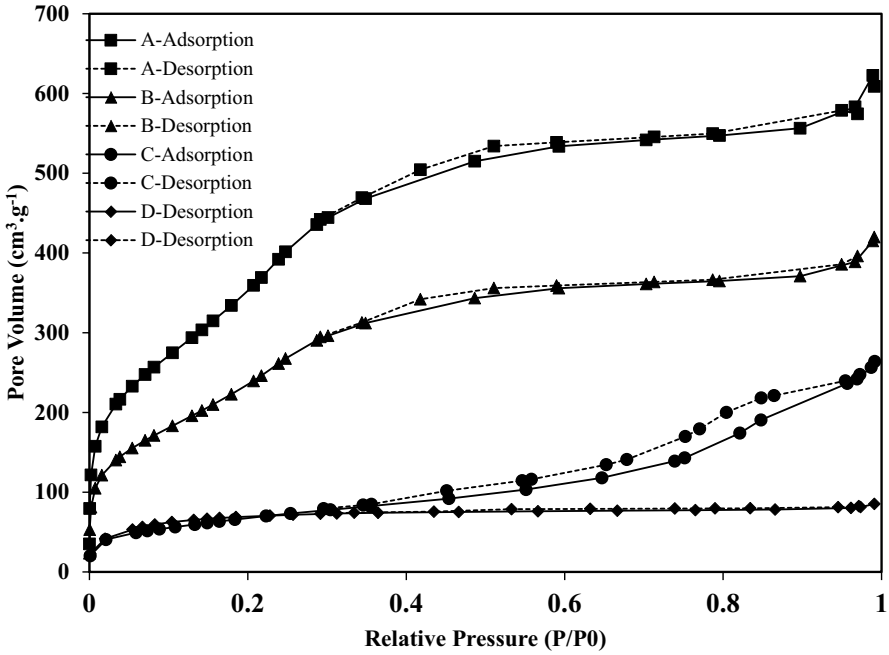

Fig. 2 N_2 adsorption/desorption plots for **a** mesoporous silica (MS) before immersion, and after immersion in **b** 0.05 M NaCl, **c** 1 M HCl, and **d** 1 M NaOH solutions

In Fig. 3, low-angle X-ray diffraction patterns of MS are shown before and after immersion in 0.05 M NaCl, 1 M HCl, and 1 M NaOH solutions. The observed (100), and (110) peaks are related to the hexagonal mesoporous silica with space group p6mm [43]. There is a peak at 2θ values of 2.16, 2.22, and 2.36° with an inter-planar d_{100} spacing of approximately 4.08, 3.97, and 3.73 nm for the as-received MS, and for powders immersed in NaCl, HCl, and NaOH. Figure 3 also displays (110) peak, illustrating more ordered hexagonal structure of MS powder before immersion in different solutions [44]. On the other hand, after immersion in acidic or alkaline solutions, only (100) peaks were detected, indicating degradation of MS at very low and high pH levels. Additionally, in the case of high-pH alkaline solution, the determined peak was not very intense, and the characteristic peak of MS had almost disappeared due to the destruction of the MS structure. MS in neutral media exhibited the highest peak intensity, indicating a lower destruction of Si–O–Si bonds, thus a minor reduction in crystallinity.

Figure 4 shows FTIR spectra of MS with and without treatment in acidic, neutral, and basic solutions. MS shows the bands at 3395 and 1604 cm^{-1} are, respectively, attributed to the stretching and bending vibrations of the adsorbed water molecules. Peaks at 1080, 795, and 455 cm^{-1} correspond to the stretching vibrations of the mesoporous framework (Si–O–Si). Moreover, the band at 960 cm^{-1} is caused by the symmetry stretching vibration of Si–OH [45]. On the other hand, the structural bonds of mesoporous silica powders exposed to neutral and acidic media did not significantly change as a result of attacking by corrosive ions in these solutions, indicating that such ions were ineffective in significantly altering the covalent bonds of MS. Nevertheless, the intensity of the Si–O–Si peak decreased in an alkaline

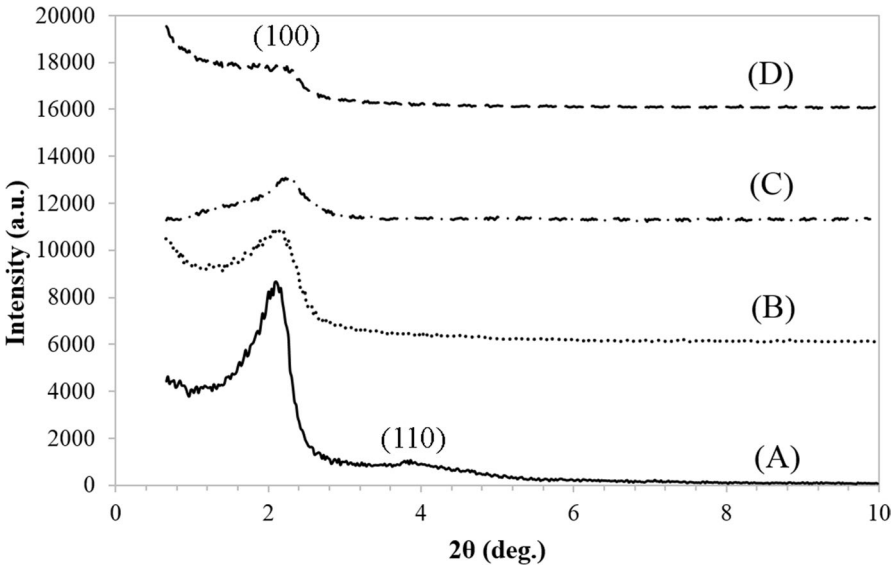

Fig. 3 XRD pattern of (**a**) mesoporous silica (MS) before immersion, and after immersion in **b** 0.05 M NaCl, **c** 1 M HCl, and **d**1 M NaOH solutions

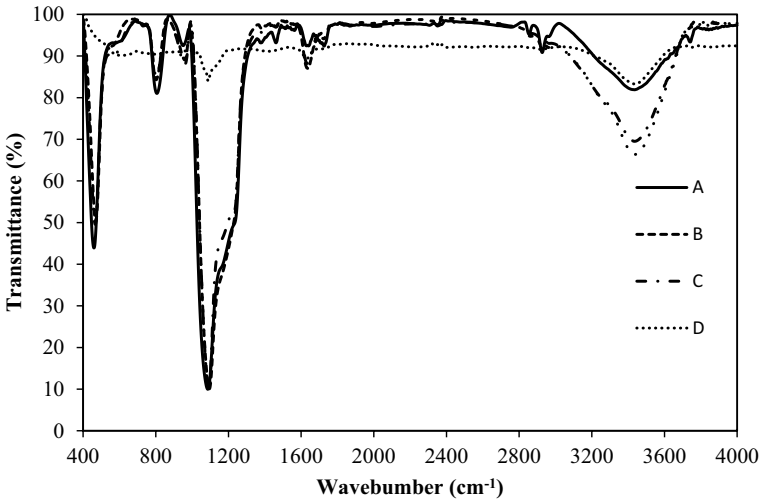

Fig. 4 FTIR spectra of **a** mesoporous silica before immersion, and after immersion in **b** 0.05 M NaCl, **c** 1 M HCl, and **d** 1 M NaOH solutions

solution due to the destruction of MS hexagonal structure. In other words, covalent bonds were strongly destroyed in the presence of hydroxyl ions.

Figure 5a–d depicts the surface micrographs of MS particles before (Fig. 5a) and after immersion in 0.05 M NaCl, 1 M HCl, and 1 M NaOH solutions. As can be observed, the morphology of MS did not change remarkably after immersion in either neutral (Fig. 5b) or acidic (Fig. 5c) media. The morphology of MS changed to spherical (Fig. 5d) after being exposed to NaOH solution, possibly due to deterioration of Si–O–Si bonds in the high-pH solution [11]. As the hydroxyl ions decompose the carrier, the corrosion inhibitor is released more quickly in alkaline media [46]. In neutral media, mesoporous silica exhibited high surface area, stable covalent bonds, high crystallinity, and unchanged morphology. Therefore, corrosion studies of mesoporous silica as a carrier were performed in neutral chloride solutions to ensure stability of mesoporous silica during the corrosion tests.

Corrosion behavior of Mes-S in the epoxy coating

Figure 6 shows electrochemical impedance spectroscopy (EIS) results for Ep, Ep/Mes, and Ep/Mes-S coatings after immersion in 0.05 M NaCl for 10 and 1000 h. These coatings showed similar capacitive behavior based on the Bode plots. Due to the barrier effect of the mesoporous silica embedded in the epoxy coating, the composite coatings had a higher impedance modulus than the blank coatings in the entire frequency range [37]. Besides, high-frequency region shows the coating response, whereas low-frequency region indicates a double-layer reaction [47]. The Ep/Mes-S coating also shows a greatest impedance magnitude ($|Z|$) and phase angle (θ) over a wide frequency range, indicating highest electrochemical resistance of this coating. The impedance magnitude ($|Z|_{100\ \mathrm{mHz}}$) of all coatings is closer together (around 1 GΩ

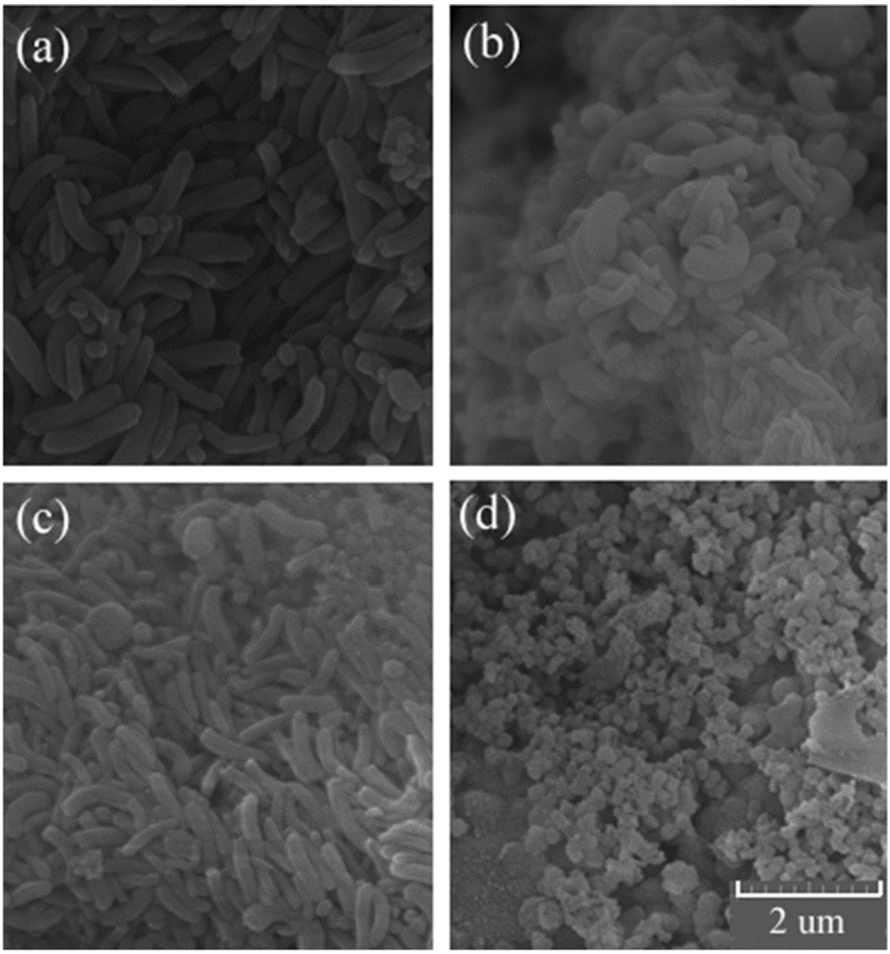

Fig. 5 FESEM micrographs of (**a**) mesoporous silica before immersion, and after immersion in **b** 0.05 M NaCl, **c** 1 M HCl, and **d** 1 M NaOH solutions

cm^2) at 10 h of immersion, while it has a highest value for Ep/Mes-S after 1000 h of immersion, suggesting the release of sulfamethazine from mesoporous silica and the development of a barrier against the diffusion of corrosive Cl^- ions [11]. Ep/Mes-S coating shows phase angle ($\theta_{10\ kHz}$) values of 89° and 64° for 10 and 1000 h, while the Ep/Mes and Ep coatings have the lower values in the same period of time, indicating a higher capacitance behavior for Ep/Mes-S due to its higher charge transfer resistance [37, 48]. Electrochemical behavior of a metal–electrolyte interface is capacitive when the charge transfer resistance and/or double-layer capacitance are high. The phase angle in this situation would be close to 90° since most of the current passes through the capacitor [4]. Accordingly, the highest phase angle of Ep/Mes-S after 10 and 1000 h of immersion indicates its high corrosion resistance to chloride media.

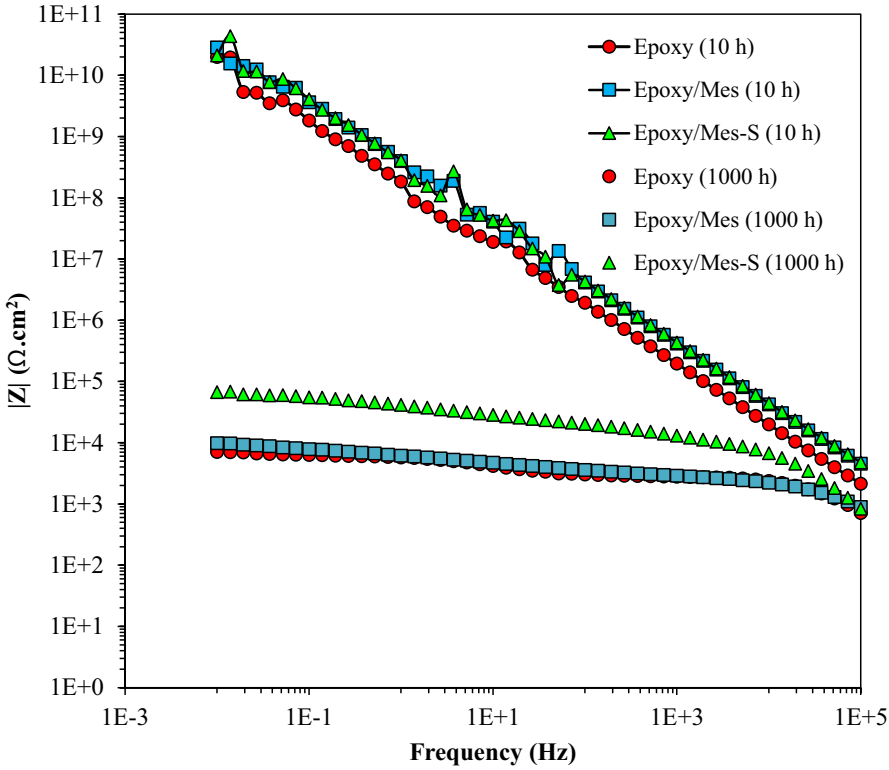

Fig. 6 Electrochemical impedance plots of Ep, Ep/Mes, and Ep/Mes-S coatings immersed in 0.05 M NaCl measured for 10 and 1000 h

Figures 7a and b illustrates the applied equivalent circuit for fitting the EIS data and determining the corrosion parameters for coatings immersed in the corrosive solution for 10 and 1000 h, respectively. In these circuits, R_s, R_{coat}, and R_{ct} refer to the solution resistance, coating resistance, and charge transfer resistance, respectively. An alternative to pure capacitance (C) is a constant phase element (CPE), which corresponds to $A^{-1}(i\omega)^{-n}$, where A is a constant number related to the interfacial capacitance, i is the complex number, ω represents the angular frequency, and n is an exponential factor which varies between -1 and 1, with a value between 0 and 1 [8]. If $n = 1$, the coating has pure capacitance behavior

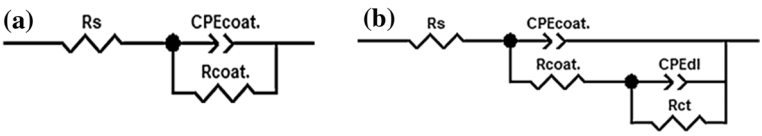

Fig. 7 The proposed equivalent circuits were utilized to calculate the corrosion resistance parameters of the produced coatings after **a** 10 h and **b** 1000 h of immersion in 0.05 M NaCl

[49]. CPE of the coatings and the double layer is denoted here as CPE_{coat} and CPE_{dl}, respectively.

Table 1 presents the corrosion parameters of the coating at different times in the chloride solution. Based on this table, the chi-squared (χ^2) values are low, indicating that EIS curve fitting is accurate [8]. Furthermore, composite coatings showed higher R_{coat} values than blank epoxy coatings, indicating the addition of mesoporous silica or Mes-S particles improved corrosion resistance. R_{coat} reduces from 1.5×10^7 to 7.3 kΩ cm^2 and from 1.1×10^7 to 2.3 kΩ cm^2 for epoxy/Mes-S and epoxy/Mes, respectively. On the other hand, R_{coat} of epoxy decreased from 8.3×10^6 to 2.1 kΩ cm^2 during this period of time. This reduction in coating resistance may be explained by the diffusion of aggressive ions into the coatings during immersion or by an increase in the number of conducting species entering the developed porosities in the coating during immersion [5, 8]. It must be noted that the R_{coat} of Ep/Mes-S coating at any time was higher than the other coating, indicating a better barrier effect due to the presence of mesoporous silica and sulfamethazine. Additionally, as time passes, CPE_{coat} increases primarily due to water permeation and ions moving through the coating [5, 37]. After 1000 h of immersion, the CPE_{coat} of Ep/Mes-S, Ep/Mes, and Ep were 4, 11, and 13 μ cm^{-2}, respectively, indicating a lower water permeation in Ep/Mes-S. Due to a lack of electrolyte diffusion, the coatings do not demonstrate R_{ct} after 10 h of immersion in the NaCl solution [50]. At 1000 h, Ep/Mes-S coatings showed the highest R_{ct} value, potentially due to the release of sulfamethazine from Mes-S particles during the corrosion. As a matter of fact, the surface adsorption of sulfamethazine released from Mes-S increases the charge transfer resistance of Ep/Mes-S coating. A further advantage of the sulfamidic group is that it is possible to increase the adsorption of the compound on mild steel surfaces by using sp^2 electron pairs on the nitrogen and oxygen atoms [36, 51]. Mild steel becomes deposited with sulfamethazine, forming a layer of adsorbed inhibitor and preventing corrosion on the surface. This adsorption layer can also be the reason for low CPE_{dl} and high R_{ct} for Ep/Mes-S [52–54].

Figure 8 shows the power spectral density (PSD) of current for the coatings immersed in the 0.05 M NaCl after 1000 h. The lower PSD (I) content for epoxy/Mes-S is indicative of its higher corrosion resistance. Low electrochemical response of the interface could be responsible for the drop in noise current measured [55]. The noise resistance (R_n) is calculated by dividing the standard deviations of voltage fluctuations by the amount of current variations [55]. Ep/Mes-S had a noise resistance of 250 kΩ cm^2, whereas Ep/Mes and Ep had noise resistances of 90 and 37 kΩ cm^2, respectively. Ep/Mes-S coating exhibited higher noise resistance due to the release of sulfamethazine in the chloride media, which blocked charge transfer reactions or diffusion of aggressive species toward the interface. In addition, the transferred charge (q) in a corrosion phenomenon can be calculated using the following equation [56]:

$$q = \frac{\sqrt{\psi_i \psi_v}}{B}. \tag{1}$$

Table 1 Corrosion parameters for Ep, Ep/Mes, and Ep/Mes-S coatings in the 0.05 M NaCl solution

Sample	Time (h)	R_{coat} (kΩ cm^2)	CPE_{coat} (μF cm^{-2})	n_{coat}	R_{ct} (kΩ cm^2)	CPE_{dl} (μF cm^{-2})	n_{dl}	Z_{100mHz} (kΩ cm^2)	θ (Deg.)	χ^2
Ep	10	8.3×10^6	4.5×10^{-3}	0.92	–	–	–	1.1×10^6	85	0.01
	1000	2.1	13	0.91	7	5.2	0.95	7	51	0.01
Ep/Mes	10	1.1×10^7	1.4×10^{-3}	0.89	–	–	–	3.7×10^6	87	0.02
	1000	2.3	11	0.91	9.8	5	0.96	7.2	60	0.005
Ep/Mes-S	10	1.5×10^7	1.1×10^{-3}	0.93	–	–	–	4.1×10^6	89	0.003
	1000	7.3	4	0.92	67	2.1	0.94	55	64	0.001

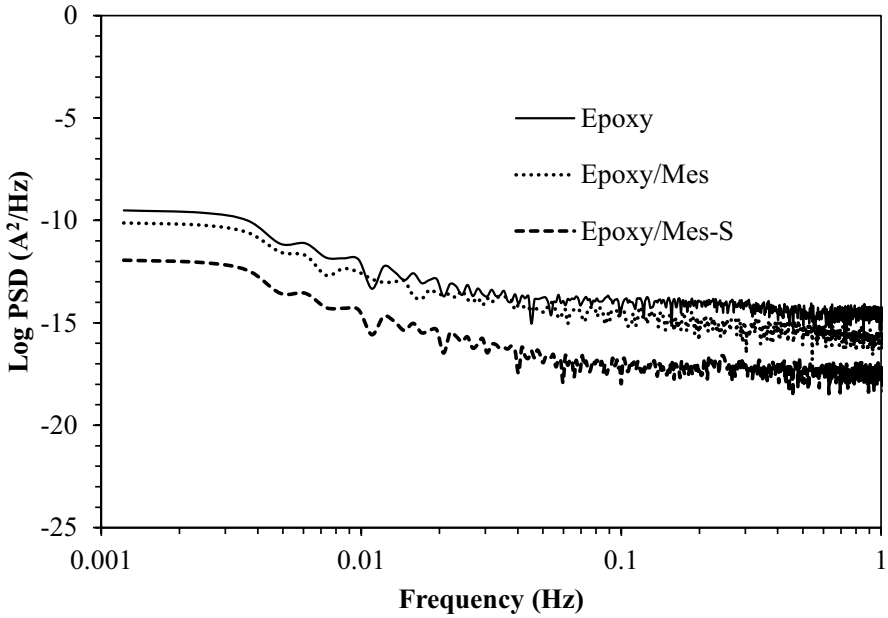

Fig. 8 Noise response of coatings after 1000 h of immersion in the 0.05 M NaCl solution

Here, Ψ_i, Ψ_v, and B represent low-frequency values of power spectrum density (PSD) (I), low-frequency values of PSD (V), and the Stern–Geary coefficient, respectively [56]. The q for the Ep/Mes-S, Ep/Mes, and Ep obtained 1.5×10^{-10}, 4.3×10^{-9}, and 5.5×10^{-9} C cm^{-2}, respectively. Hence, the Ep/Mes-S coating provides higher protection because of the release of sulfamethazine from the mesoporous silica particles, resulting in lower charge transferred across the interface.

Figure 9a shows the surface micrograph of the scratched zone of the Ep/Mes-S coating together with the line scan of sulfur element demonstrating the presence of S and the release of sulfamethazine in the scratched area where the coating was corroding in the 0.05 M NaCl solution. Figure 9b shows the XPS spectrum of the scratched area after the immersion. In the XPS analysis, a S_{2p} peak at about 163 eV was detected due to sulfamethazine adsorption on the surface of mesoporous silica [57, 58]. It is believed that the presence of lone sp^2 electron pairs of heterocyclic rings and the sulfamidic functional group in sulfamethazine enhances the adsorption process onto carbon steel surfaces [36]. Other detected peaks (Fe_{2p}, O_{1s}, and C1s) can be related to the carbon steel and oxidation process during the immersion in the corrosive media.

Figure 10a shows the fluorescence images of *E. coli* for identification after exposure on the surface of Ep, Ep/Mes, and Ep/Mes-S coatings. Due to high surface area of mesoporous silica, epoxy containing Mes has a greater antibacterial effect than blank epoxy, since mesoporous silica was found to have antibacterial properties against E. coli [59]. It was found that the Ep/Mes-S displayed the highest level of antibacterial activity. As mentioned earlier, sulfamethazine has antibacterial

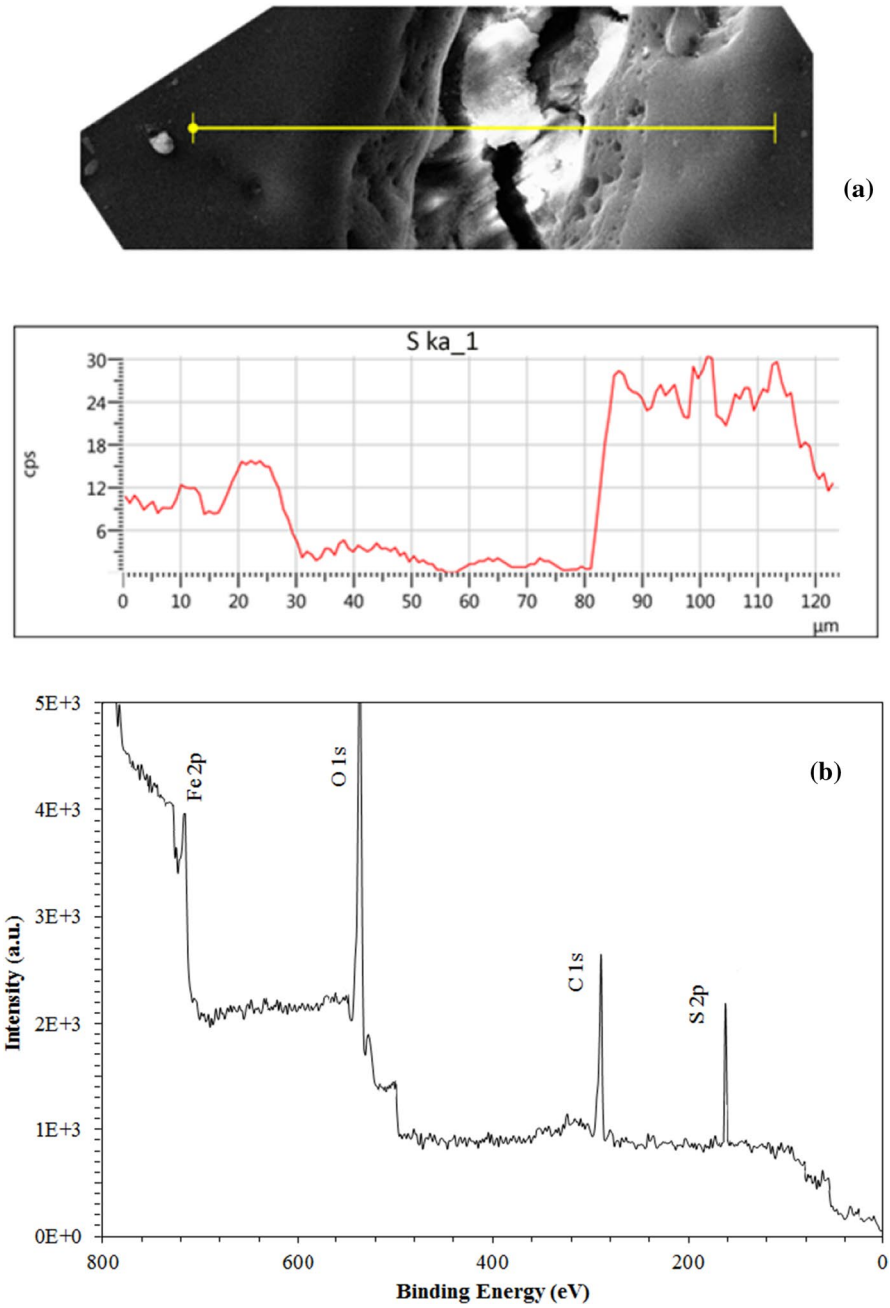

Fig. 9 **a** SEM micrograph and EDS line scan of sulfur. **b** XPS spectrum of the scratched surface of Ep/Mes-S coating

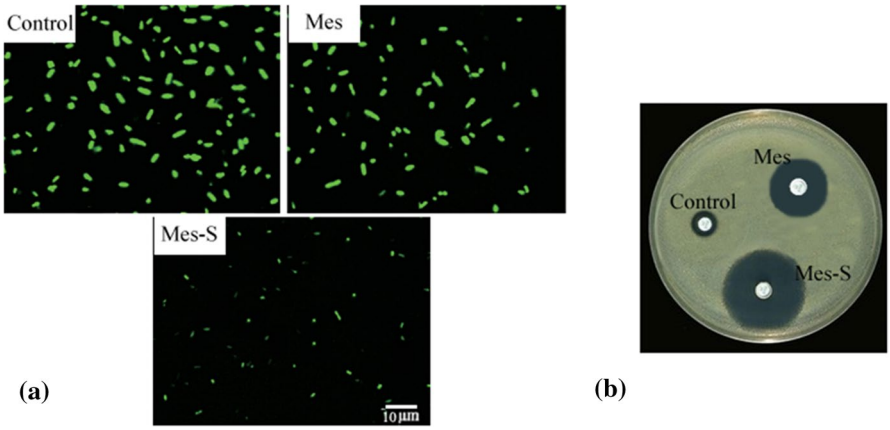

Fig. 10 **a** Fluorescent microscopy of the coatings exposing to *E. coli* and **b** disk diffusion test results for Mes and Mes-S powders

properties, which inhibits the growth of *E. coli* [28, 32]. The $–SO_2$ group in the molecule structure can explain the reaction rate of this antibacterial inhibitor [60]. This type of drug can act as competitive inhibitors of the enzyme dihydropteroate synthase, and, therefore, these are bacteriostatic and inhibit the growth and multiplication of bacteria [61]. Figure 10b shows the results of the disk diffusion test, indicating a higher inhibition zone for Mes-S. The measured inhibition zone for the control, Mes, and Mes-S samples were about 10, 24, and 30 mm, respectively. The most significant inhibition zone associated with Mes-S may result from sulfamethazine's antibacterial properties. Sulfamethazine or its ions can release from the Mes-S through the mesoporous channels and interact with bacteria or high local concentration of sulfamethazine on surface of mesoporous silica interact with the bacterial cell walls and consequently cause cell membrane damage [62].

Conclusions

This study examined the corrosion and antibacterial properties of epoxy coatings containing mesoporous silica loaded with sulfamethazine. According to the results, sulfamethazine acts both as a corrosion inhibitor and an antibacterial agent. When released from the mesoporous silica, it reacts with the surface by linking sulfamethazine sp^2 electron pairs and iron atoms. During the corrosion process, S-containing compounds adsorb onto the surface of mild steel, which results in the greater charge transfer resistance of Ep/Mes-S than Ep/Mes. Also, the coating with Mes-S showed the highest level of antibacterial effect due to the presence of sulfamethazine. By interacting with the bacterial cell wall, it damages the cell membrane.

Acknowledgements This study was financially supported by Shahid Chamran University of Ahvaz with the Grant Number of SCU.EM1400.31395.

Declarations

Conflict of interest The authors declare that they have no known competing financial interests or personal relationships that could have appeared to influence the work reported in this paper.

References

1. Makhlouf ASF (ed) (2014) Preface. Handbook of Smart Coatings Mater. Prot. Woodhead Publishing, UK, p 656. https://doi.org/10.1016/B978-0-85709-680-7.50027-9.
2. Lyon SB, Bingham R, Mills DJ (2017) Progress in organic coatings advances in corrosion protection by organic coatings: What we know and what we would like to know. Prog Org Coatings 102:2–7. https://doi.org/10.1016/j.porgcoat.2016.04.030
3. Song B, Shi Y, Liu Q (2020) An inorganic route to decorate graphene oxide with nanosilica and investigate its effect on anti-corrosion property of waterborne epoxy. Polym Adv Technol 31:309–318. https://doi.org/10.1002/pat.4770
4. Keyvani A, Yeganeh M, Rezaeyan H (2017) Application of mesoporous silica nanocontainers as an intelligent host of molybdate corrosion inhibitor embedded in the epoxy coated steel. Prog Nat Sci Mater Int 27:261–267. https://doi.org/10.1016/j.pnsc.2017.02.005
5. Yeganeh M, Keyvani A (2016) The effect of mesoporous silica nanocontainers incorporation on the corrosion behavior of scratched polymer coatings. Prog Org Coatings 90:296–303. https://doi.org/10.1016/j.porgcoat.2015.11.006
6. Zadeh MK, Yeganeh M, Shoushtari MT, Esmaeilkhanian A (2021) Corrosion performance of polypyrrole-coated metals: a review of perspectives and recent advances. Synth Met 274:116723. https://doi.org/10.1016/j.synthmet.2021.116723
7. Shahryari Z, Yeganeh M, Gheisari K, Ramezanzadeh B (2021) A brief review of the graphene oxide-based polymer nanocomposite coatings: preparation, characterization, and properties. J Coatings Technol Res, pp 1–25. https://doi.org/10.1007/s11998-021-00488-8.
8. Saremi M, Yeganeh M (2014) Application of mesoporous silica nanocontainers as smart host of corrosion inhibitor in polypyrrole coatings. Corros Sci 86:159–170. https://doi.org/10.1016/j.corsci.2014.05.007
9. Rajendran S, Nguyen TA, Kakooei S, Yeganeh M (2020) Corrosion protection at the nanoscale. Elsevier, Amsterdam.
10. Stankiewicz A, Szczygieł I, Szczygieł B (2013) Self-healing coatings in anti-corrosion applications. J Mater Sci 48:8041–8051. https://doi.org/10.1007/s10853-013-7616-y
11. Yeganeh M, Nguyen TA, Rajendran S, Kakooei S, Li Y (2020) Chapter 1—Corrosion protection at the nanoscale: an introduction. In: Rajendran S, Nguyen TANH, Kakooei S, Yeganeh M, Li Y (eds) Corros. Prot. Nanoscale. Elsevier, Amsterdam, 3–7. https://doi.org/10.1016/B978-0-12-819359-4.00001-5.
12. Abu-Thabit NY, Hamdy AS (2016) Stimuli-responsive Polyelectrolyte Multilayers for fabrication of self-healing coatings—a review. Surf Coatings Technol 303:406–424. https://doi.org/10.1016/j.surfcoat.2015.11.020
13. Zahidah KA, Kakooei S, Ismail MC, Bothi Raja P (2017) Review. Prog Org Coatings 111:175–185. https://doi.org/10.1016/j.porgcoat.2017.05.018.
14. Shchukin DG, Möhwald H (2011) Smart nanocontainers as depot media for feedback active coatings. Chem Commun 47:8730–8739. https://doi.org/10.1039/C1CC13142G
15. Jain P, Patidar B, Bhawsar J (2020) Potential of nanoparticles as a corrosion inhibitor : a review. J Bio- Tribo-Corrosion 6:1–12. https://doi.org/10.1007/s40735-020-00335-0
16. Nguyen TA, Assadi AA (2018) Smart nanocontainers: preparation, loading/release processes and applications. Kenkyu J Nanotechnol Nanosci 4:2–7. https://doi.org/10.31872/2018/kjnn-s1-100101.
17. Liu X, Li W, Wang W, Song L, Fan W, Gao X, Xiong C (2018) Synthesis and characterization of pH-responsive mesoporous chitosan microspheres loaded with sodium phytate for smart water-based coatings. Mater Corros 69:736–748. https://doi.org/10.1002/maco.201709840
18. Sargazi S, Laraib U, Barani M, Rahdar A, Fatima I, Bilal M, Pandey S, Sharma RK, Kyzas GZ (2022) Recent trends in the mesoporous silica nanoparticles with rode-like morphology for cancer theranostics: a review. J Mol Struct 1261:132922. https://doi.org/10.1016/j.molstruc.2022.132922

19. Yu L, Yao L, Yang K, Fei W, Chen Q, Qin L, Liu S, Cao M, Liu Q, Qin B (2022) cRGD-modified core–shell mesoporous silica@BSA nanoparticles for drug delivery. Polym Bull In press. https://doi.org/10.1007/s00289-021-03999-x
20. Kurinchyselvan S, Chandramohan A, Hariharan A, Gomathipriya P, Alagar M (2021) Mesoporous silica MCM-41-reinforced cardanol-based benzoxazine nanocomposites for low-k applications. Polym Bull 78:2043–2065. https://doi.org/10.1007/s00289-020-03198-0
21. Borisova D, Möhwald H, Shchukin DG (2011) Mesoporous silica nanoparticles for active corrosion protection. ACS Nano 5:1939–1946. https://doi.org/10.1021/nn102871v
22. Falcón JM, Otubo LM, Aoki IV (2016) Highly ordered mesoporous silica loaded with dodecylamine for smart anticorrosion coatings. Surf Coatings Technol 303:319–329. https://doi.org/10.1016/j.surfcoat.2015.11.029
23. Changjean W, Huang L, Liu P, Tsai T (2014) Microporous and mesoporous materials repairable mesoporous silica film with replenishing corrosion inhibitor as corrosion protection layer of aluminum alloy. MICROPOROUS MESOPOROUS Mater. https://doi.org/10.1016/j.micromeso.2014.02.030
24. Qiao Y, Li W, Wang G, Zhang X, Cao N (2015) Application of ordered mesoporous silica nanocontainers in an anticorrosive epoxy coating on a magnesium alloy surface. RSC Adv 5:47778–47787. https://doi.org/10.1039/C5RA05266A
25. Noiville R, Jaubert O, Gressier M, Bonino J, Taberna P, Fori B, Menu M, Noiville R, Jaubert O, Gressier M, Bonino J, Taberna P (2019) Ce (III) corrosion inhibitor release from silica and boehmite nanocontainers To cite this version: HAL Id : hal-02020913. Mater Sci Eng B 229:144–154
26. Rahsepar M, Mohebbi F, Hayatdavoudi H (2017) Synthesis and characterization of inhibitor-loaded silica nanospheres for active corrosion protection of carbon steel substrate. J Alloys Compd 709:519–530. https://doi.org/10.1016/j.jallcom.2017.03.104
27. Yeganeh M, Omidi M, Mortazavi SHH, Etemad A, Nazari MH, Marashi SM (2020) Application of mesoporous silica as the nanocontainer of corrosion inhibitor. Elsevier Inc., Amsterdam. https://doi.org/10.1016/b978-0-12-819359-4.00015-5.
28. El-Naggar MM (2007) Corrosion inhibition of mild steel in acidic medium by some sulfa drugs compounds. Corros Sci 49:2226–2236. https://doi.org/10.1016/j.corsci.2006.10.039
29. Mrani SA, Arrousse N, Haldhar R, Lahcen AA, Amine A, Saffaj T, Kim S, Taleb M (2022) In Silico approaches for some sulfa drugs as eco-friendly corrosion inhibitors of iron in aqueous medium. Lubricants 10:1–12
30. Bagdatli E, Cil E (2022) Sulfa drugs–based Norbornenyl imides and reductive Heck reactions: synthesis and antimicrobial screening. J Heterocycl Chem 59:264–274. https://doi.org/10.1002/jhet.4380
31. Lin Y, Zhou M, Wang G, Li H, Wei Y, Lou Y, Zhang D, Ji L (2022) Degradation and transformation pathways of sulfamethazine by pre-oxidation disinfection process. J Environ Chem Eng 10:1–10. https://doi.org/10.1016/j.jece.2022.107194
32. Zhang L, Shen S (2020) Adsorption and catalytic degradation of sulfamethazine by mesoporous carbon loaded nano zero valent iron. J Ind Eng Chem 83:123–135
33. Carucci C, Scalas N, Porcheddu A, Piludu M, Monduzzi M, Salis A (2021) Adsorption and release of sulfamethizole from mesoporous silica nanoparticles functionalised with triethylenetetramine. Int J Mol Sci 22:7665. https://doi.org/10.3390/ijms22147665
34. Conde-Cid M, Cela-Dablanca R, Ferreira-Coelho G, Fernández-Calviño D, Núñez-Delgado A, Fernández-Sanjurjo MJ, Arias-Estévez M, Álvarez-Rodríguez E (2021) Sulfadiazine, sulfamethazine and sulfachloropyridazine removal using three different porous materials: Pine bark, “oak ash” and mussel shell. Environ Res 195:110814. https://doi.org/10.1016/j.envres.2021.110814
35. Hussain I, Li Y, Qi J, Li J, Sun X, Shen J, Han W, Wang L (2018) Synthesis of magnetic yolk-shell mesoporous carbon architecture for the effective adsorption of sulfamethazine drug. Microporous Mesoporous Mater 255:110–118. https://doi.org/10.1016/j.micromeso.2017.07.027
36. Yeganeh M, Asadi N, Omidi M, Mahdavian M (2019) An investigation on the corrosion behavior of the epoxy coating embedded with mesoporous silica nanocontainer loaded by sulfamethazine inhibitor. Prog Org Coatings, 128. https://doi.org/10.1016/j.porgcoat.2018.12.022.
37. Yeganeh M, Saremi M (2015) Corrosion inhibition of magnesium using biocompatible Alkyd coatings incorporated by mesoporous silica nanocontainers. Prog Org Coatings 79:25–30. https://doi.org/10.1016/j.porgcoat.2014.10.015

38. Saremi M, Yeganeh M (2010) Investigation of corrosion behaviour of nanostructured copper thin film produced by radio frequency sputtering, Micro. Nano Lett 5:70–75. https://doi.org/10.1049/mnl.2009.0111
39. Vazquez NI, Gonzalez Z, Ferrari B, Castro Y (2017) Synthesis of mesoporous silica nanoparticles by sol–gel as nanocontainer for future drug delivery applications, Boletín La Soc. Española Cerámica y Vidr 56:139–145. https://doi.org/10.1016/j.bsecv.2017.03.002
40. Brijitta J, Ramachandran D, Rabel AM, Raj NN, Viswanathan K, Prasath SS (2017) Evolution of shape isotropy in silica microparticles induced by the base. Colloid Polym Sci 295:1485–1490. https://doi.org/10.1007/s00396-017-4118-5
41. Cychosz KA, Thommes M (2018) Progress in the Physisorption Characterization of Nanoporous Gas Storage Materials. Engineering 4:559–566. https://doi.org/10.1016/j.eng.2018.06.001
42. Yeganeh M, Omidi M, Rabizadeh T (2019) Anti-corrosion behavior of epoxy composite coatings containing molybdate- loaded mesoporous silica. Prog Org Coatings 126:18–27. https://doi.org/10.1016/j.porgcoat.2018.10.016
43. Zhang H, Liu S (2018) Synthesis of ordered cubic smaller supermicroporous mesoporous silica using ionic liquid as template. Mater Lett 221:119–122. https://doi.org/10.1016/j.matlet.2018.03.118
44. Chen C-C, Do J-S, Gu Y (2009) Immobilization of HRP in Mesoporous Silica and Its Application for the Construction of Polyaniline Modified Hydrogen Peroxide Biosensor. Sensors 9:4635–4648. https://doi.org/10.3390/s90604635
45. Sun J, Zhang C, Zhang C, Ding R, Xu Y (2014) Effect of post-treatment on ordered mesoporous silica antireflective coating. RSC Adv 4:50873–50881. https://doi.org/10.1039/C4RA06788F
46. Chen T, Fu J (2012) {pH}-responsive nanovalves based on hollow mesoporous silica spheres for controlled release of corrosion inhibitor. Nanotechnology 23:235605. https://doi.org/10.1088/0957-4484/23/23/235605
47. Yeganeh M, Rezvani MH, Laribaghal SM (2021) Electrochemical behavior of additively manufactured 316 L stainless steel in H2SO4 solution containing methionine as an amino acid. Colloids Surfaces A Physicochem Eng Asp 627:127120. https://doi.org/10.1016/j.colsurfa.2021.127120
48. Mahdavian M, Ashhari S (2010) Corrosion inhibition performance of 2-mercaptobenzimidazole and 2-mercaptobenzoxazole compounds for protection of mild steel in hydrochloric acid solution. Electrochim Acta 55:1720–1724. https://doi.org/10.1016/j.electacta.2009.10.055
49. Keyvani A, Yeganeh M, Rezaeyan H (2017) Electrodeposition of Zn-Co-Mo Alloy on the Steel Substrate from Citrate Bath and Its Corrosion Behavior in the Chloride Media. J Mater Eng Perform 26:1958–1966. https://doi.org/10.1007/s11665-017-2619-5
50. Lu F, Song B, He P, Wang Z, Wang J (2017) Electrochemical impedance spectroscopy (EIS) study on the degradation of acrylic polyurethane coatings. RSC Adv 7:13742–13748. https://doi.org/10.1039/c6ra26341k
51. Arslan T, Kandemirli F, Ebenso EE, Love I, Alemu H (2009) Quantum chemical studies on the corrosion inhibition of some sulphonamides on mild steel in acidic medium. Corros Sci 51:35–47. https://doi.org/10.1016/j.corsci.2008.10.016
52. Perez N (2016). Electrochemistry and Corrosion Science. https://doi.org/10.1007/978-3-319-24847-9
53. Naderi R, Attar MM (2014) Effect of zinc-free phosphate-based anticorrosion pigment on the cathodic disbondment of epoxy-polyamide coating. Prog Org Coatings, pp 77. https://doi.org/10.1016/j.porgcoat.2014.01.012.
54. Bagherzadeh MR, Mahdavi F (2007) Preparation of epoxy–clay nanocomposite and investigation on its anti-corrosive behavior in epoxy coating. Prog Org Coatings PROG ORG Coat 60:117–120. https://doi.org/10.1016/j.porgcoat.2007.07.011
55. Yeganeh M, Omidi M, Rabizadeh T (2019) Anti-corrosion behavior of epoxy composite coatings containing molybdate-loaded mesoporous silica. Prog Org Coatings, 126. https://doi.org/10.1016/j.porgcoat.2018.10.016.
56. Markhali BP, Naderi R, Mahdavian M, Sayebani M, Arman SY (2013) Electrochemical impedance spectroscopy and electrochemical noise measurements as tools to evaluate corrosion inhibition of azole compounds on stainless steel in acidic media. Corros Sci 75:269–279. https://doi.org/10.1016/j.corsci.2013.06.010
57. Al-Fakih AM, Abdallah HH, Aziz M (2019) Experimental and theoretical studies of the inhibition performance of two furan derivatives on mild steel corrosion in acidic medium. Mater Corros 70:135–148. https://doi.org/10.1002/maco.201810221

58. Yeganeh M, Khosravi-Bigdeli I, Eskandari M, Zaree SRA (2020) corrosion inhibition of L-methionine amino acid as a green corrosion inhibitor for stainless steel in the H2SO4 solution. J Mater Eng Perform 29:3983–3994. https://doi.org/10.1007/s11665-020-04890-y
59. Park S-Y, Barton M, Pendleton P (2011) Mesoporous silica as a natural antimicrobial carrier. Colloids Surfaces A Physicochem Eng Asp 385:256–261. https://doi.org/10.1016/j.colsurfa.2011.06.021
60. Uslu MO, Balcioglu IA (2009) Simultaneous removal of oxytetracycline and sulfamethazine antibacterials from animal waste by chemical oxidation processes. J Agric Food Chem 57:11284–11291. https://doi.org/10.1021/jf902188j
61. Madigan MT (2015) Brock biology of microorganisms/Michael T. Madigan, Southern Illinois University Carbondale; John M. Martinko, Southern Illinois University Carbondale; Kelly S. Bender Southern Illinois University Carbondal; Daniel H. Buckley, Cornell University ; D, Fourteenth, Pearson, Boson, 2015.
62. Liu J, Li S, Fang Y, Zhu Z (2019) Boosting antibacterial activity with mesoporous silica nanoparticles supported silver nanoclusters. J Colloid Interface Sci 555:470–479. https://doi.org/10.1016/j.jcis.2019.08.009